Quenching of the $2pnd\ ^1P^o$ doubly excited states of helium by a dc electric field

K. Bučar,* M. Žitnik, and A. Mihelič
Jožef Stefan Institute, Jamova cesta 39, SI-1001 Ljubljana, Slovenia

F. Penent, P. Lablanquie, J. Palaudoux, and L. Andrić
UPMC, Université Paris 06, LCPMR, 11 rue Pierre et Marie Curie, 75231 Paris Cedex 05, France
and CNRS, LCPMR (UMR 7614), 11 rue Pierre et Marie Curie, 75231 Paris Cedex 05, France

M. Braune
Fritz-Haber-Institut der Max-Planck-Gesellschaft, 14195 Berlin, Germany

R. Püttner
Institut für Experimentalphysik, Freie Universität Berlin, Arnimallee 14, D-14195 Berlin-Dahlem, Germany
(Received 17 April 2014; published 11 July 2014)

The fluorescence yield quenching of low-lying doubly excited $2pnd\ ^1P^o$ states is observed to depend strongly on a dc electric field strength and its orientation with respect to the polarization of the incoming photon beam. The reduction of the yield accompanied by the lifetime shortening is attributed to the Stark mixing with the neighboring $2sns\ ^1S^e$ states, which redirects the $2pnd\ ^1P^o$ decay to the prompt autoionization channel. For $n \geqslant 4$, the lifetimes decrease from several hundred picoseconds down to several tens of picoseconds when an electric field in the kV/cm range is applied parallel to the photon probe polarization. Practically no lifetime change is observed for polarization perpendicular to the electric field direction. The results of the complex-scaling calculations are in a good agreement with the experimental data.

DOI: 10.1103/PhysRevA.90.013412 PACS number(s): 32.60.+i, 32.70.Cs

I. INTRODUCTION

Helium doubly excited states are a test bed for electron correlation studies in three-body systems. After the culmination of high-resolution photoionization studies in the 1990s [1,2], the observation of the fluorescence decay channel [3,4] has triggered new experimental possibilities. Besides direct spectroscopic investigation of the corresponding emission in the vacuum ultraviolet (VUV) and in the visible energy range [5–7], an extremely efficient detection of metastable helium atoms made it possible to quantify the violation of the LS-coupling approximation in helium [8–12], and effects of homogeneous magnetic [13] and electric fields [14–16] on doubly excited states (DES) below $N = 2$ ionization threshold were investigated.

For the majority of the DES, the direct spectroscopic determination of the natural linewidths and of the tiny, field-induced line shifts is not possible because, at present, the energy resolution of photon sources in the VUV region cannot reach the required μeV range [17]. On the other hand, the resonance lifetime variations of the order of tens of picoseconds can readily be observed in the time domain by relying on the pulsed structure of the synchrotron light sources. The time-resolved fluorescence detection was employed to study the $2pnd\ ^1P^o$ DES series [18–20]. The successful measurements of ≈200-ps-long lifetimes under single-bunch synchrotron operation initiated time-resolved studies in the multibunch operation mode to increase the experimental efficiency. In general, below the $N = 2$ threshold there are two $^1S^e$, three $^1P^o$, one $^1P^e$, one $^1D^o$, and three $^1D^e$ Rydberg series. From these in the field-free case only the three $^1P^o$ series are dipole allowed. In the nonzero electric field environment neither the total angular momentum L nor the parity π are good quantum numbers anymore. As a result, the above-mentioned series are allowed to mix. Because this is in the presence of an electric field, the signal of the so-called "dark" (dipole-forbidden) $2pnp\ ^1P^e$ states ($n = 7$–10) was observed in the fluorescence spectra [16]. Investigations of these parity-forbidden states in the time domain relate the observed decrease of the lifetime to the Stark admixture of the autoionizing $^1P^o$ DES [21]. In detail it was demonstrated that the visibility and the lifetime of the $2pnp\ ^1P^e$ states crucially depend on the electric field strength and on its direction with respect to the incoming photon polarization.

In this paper we present a complementary study of the strong, Stark-induced quenching of the "visible" (dipole-allowed) DES $2pnd\ ^1P^o$ ($n = 3$–7). We have set up a measurement in the picosecond time domain to determine the lifetimes of these DES in a homogeneous dc electric field. Under the field-free conditions, these states, which are conventionally labeled with the letter c [22] or with the $(K,T)^A = (-1,0)^0$ correlation quantum numbers [23,24], are relatively long lived: Although autoionization for these states is not forbidden, they primarily decay by fluorescence to the singly excited states [25]. However, the neighboring members of the two strongly autoionizing $2sns$ and $2pnp\ ^1S^e$ series—labeled with the letters a and b or with $(K,T)^A = (1,0)^+$ and $(K,T)^A = (-1,0)^+$—can mix at low electric field strengths with the $nc\ ^1P^o$ states. The system presented below is interesting also because the mixing is expected to depend strongly on the relative angle between the electric field $\mathbf{F}$ and the photon polarization direction $\hat{\mathbf{e}}_0$. We choose the quantization (z) axis to be parallel to the electric field, i.e., $\mathbf{F} \parallel \hat{\mathbf{z}}$. In the perpendicular

*klemen.bucar@ijs.si

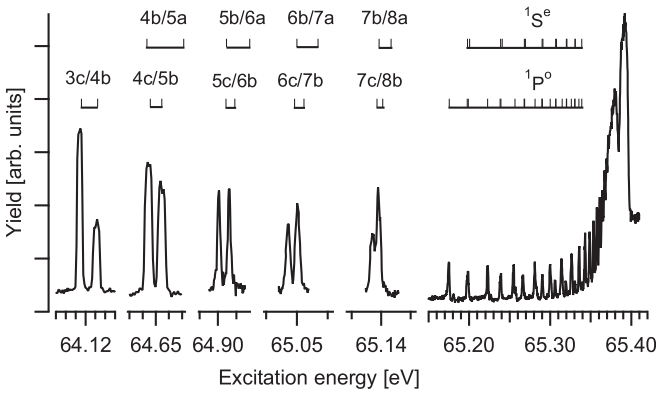

FIG. 1. Fluorescence yield measured in the region of $nc/(n+1)b$ $^1P^o$ doublets below the $N=2$ threshold. Denoted are also the energy positions of the dark $nb/(n+1)a$ $^1S^e$ doublets. The energy axes are expanded so that each minor tick represents 10 meV. The experimental energies have been shifted by 20 meV to match the calculated energy positions. Each doublet was measured under different experimental conditions and the yields are not given on the same scale.

geometry, when $\mathbf{F} \perp \hat{\mathbf{e}}_0$, only DES with $m_L = \pm 1$ projection of the angular momentum on the direction of the external field are accessible in the ground-state photoabsorption [26]. As these states cannot mix with the unperturbed $^1S^e$ states, which all have $m_L = 0$, no measurable effect on the lifetime of $^1P^o$ states is expected when an external electric field is applied. Conversely, when $\mathbf{F} \parallel \hat{\mathbf{e}}_0$, the $m_L = 0$ states are accessible and the lifetime variation of nc $^1P^o$ states is expected to be the largest. Although the field-induced mixing affects also the nb and $(n+1)a$ $^1S^e$ resonances, these states are not expected to be directly visible in the fluorescence spectrum because of their strong autoionizing character and due to the strong experimental overlap with the other DES (Fig. 1). Their presence, however, is indicated indirectly by the behavior of the nc $^1P^o$ states as a function of the field strength, as can be seen through the decrease of the corresponding fluorescence yield in the energy domain and through the lifetime shortening in the time domain.

The fluorescence spectra reported in the past were "contaminated" by Fano-like signal, which originates from the main autoionizing na $^1P^o$ series due to secondary ultraviolet (UV) photons generated by a plethora of emitted electrons hitting surfaces [16]. This effect, as well as the contribution of another UV photon emitted along the cascade decay (from the $1s2p \rightarrow 1s^2$ transition), prevents a precise quantitative analysis of the fluorescence yield quenching, which is a consequence of the coupling with the dark states. In a time-resolved measurement, both the electron contamination signal and the contribution from the second UV photon result in a flat background, and the effect of the resonance Stark mixing is clearly reflected in the field-dependent nc $^1P^o$ lifetime.

II. EXPERIMENT

The measurements were performed at the U56/2-PGM1 BESSY II beamline in Berlin in the multibunch operation mode with 2-ns period between the light pulses. The optimized energy resolution of the photon beam was about 0.8 meV (resolving power 80 000) (Fig. 1). The experimental setup is

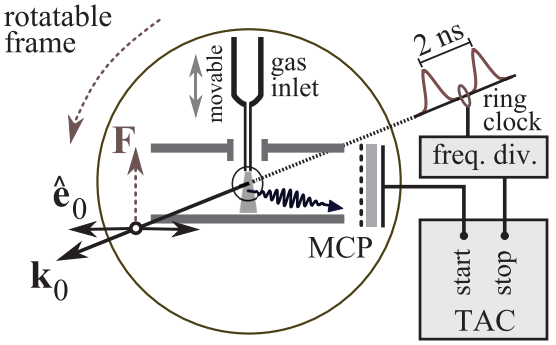

FIG. 2. (Color online) The experimental scheme. The direction of external electric field $\mathbf{F}$ can be rotated around the wave vector $\mathbf{k}_0$ of the incident photon beam to change its angle with respect to the incoming light polarization $\hat{\mathbf{e}}_0$.

similar to the one described in Ref. [21] with the exception that here the gas inlet, the two coplanar electrodes, and the 40-mm microchannel plate (MCP) detector are mounted on a frame which can be rotated around the direction of the incoming photon beam (Fig. 2). A dc electric field $\mathbf{F}$ with strength up to 4 kV/cm is applied in the target region at the crossing of the effusive helium jet with the polarized synchrotron light beam. A numerical simulation of the field strength suggested a value in the interaction region as 90% of the nominal (geometrical) one for the parallel plate arrangement [21], and such a correction is applied throughout this paper. The field direction with respect to the photon polarization was set by a frame rotation without changing the detection solid angle. The fluorescence signal from selectively excited resonances was detected by the MCP equipped with voltage-biased grids to avoid detection of charged particles. The signal processed by fast timing electronics (1 GHz preamplifier and constant-fraction discriminator) was sent as START to a time-to-amplitude converter (TAC) which was stopped by the frequency-divided ($\div 32$) rf signal (giving a 64-ns period). The TAC time window was set to 50 ns. The TAC output was digitized by an analog-to-digital converter (ADC) with 2K channels giving a final bin width in the time spectrum of 25 ps or lower (6 ps with 8K channels). The TAC stop signal period of 64 ns with a ring period of 800 ns ensures that the signal from all light bunches is averaged on two cycles (2×800 ns $=$ 25×64 ns). Besides the frame rotation, a translation of the gas inlet (needle) with respect to the frame was possible. That feature was introduced to measure the instrumental temporal resolution of the system: The instrumental function $I(t)$ was determined by inserting the tip of the needle into the "edges" of the photon beam to avoid saturation of the signal and recording the time spectrum of scattered photons with respect to the ring clock [solid line in Fig. 3(a)]. The shape of the instrumental function can be approximately described by a Gaussian with a typical full width at half maximum (FWHM) of 120 ps.

A. Deconvolution

The fluorescence rate at the observed time depends on the population and on the decay time of the excited state (see Fig. 4). The fluorescence rate $F(t)$ detected at time t is therefore described by a convolution of the excitation

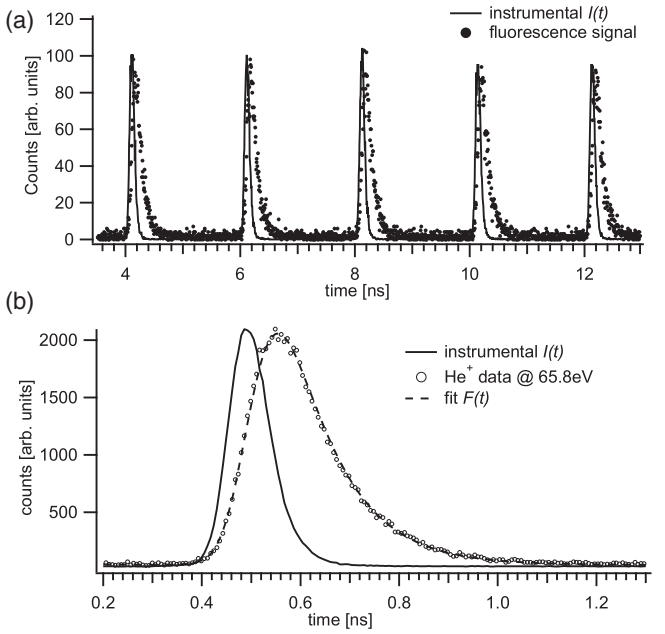

FIG. 3. Benchmark determination of the lifetime of the He^+ $2p$ state in the zero electric field. Shown are the multibunch signal (a) and the signal of many bunches folded into an equivalent single-bunch response (b).

rate E with an exponential decay function D and time jitter G_1: $F(t) \propto (E * D * G_1)(t)$. Measuring the scattered photons from the needle is described in a similar way, but without the exponential decay: $I(t) \propto (E * G_2)(t - \Delta t_0)$. Note that a different time jitter function G_2 has been used due to a different data acquisition time and that an additional time shift Δt_0 has been introduced to account for the difference in the photon paths because the beam "edges" which provide the signal on the needle do not obey the focusing conditions (position and time) of the central part of the beam. Furthermore, a small amount of light scattered from the needle was detected even when the needle was moved out of the beam. This adds a term proportional to $(E * G_1)(t - \Delta t_1)$ to the measured signal, where Δt_1 is the time shift related to the needle-out position. When this term is small and the time jitter G_1 is similar to G_2, we can approximate it with the shifted measured instrumental function $I(t)$, normalized to the acquisition time and to the incident photon flux. In this case, the expected fluorescence signal is

$$F(t) = Y \int I(t' - \Delta t_0)\,(G_0 * D)(t - t', \sigma_0, \tau)\,dt' + \alpha \int I(t' - \Delta t_1) G_0(t - t', \sigma_0)\,dt'. \quad (1)$$

The parameter σ_0 describes an additional broadening of G_1 with respect to G_2, so that $G_2 * G_0 = G_1$. The decay signal $(G_0 * D)(t, \sigma_0, \tau)$ is described by a convolution of an exponential with a Gauss-shaped time-jitter correction [27]:

$$(G_0 * D)(t, \tau, \sigma_0) = \frac{1}{\sqrt{2\pi}\sigma_0 \tau} \times \int_{-t}^{\infty} \exp\left(-\frac{t'^2}{2\sigma_0^2} - \frac{t' + t}{\tau}\right) dt'. \quad (2)$$

Parameter Y is proportional to the fluorescence yield meditated by the resonant photoabsorption. To implement the fitting of the continuous and possibly subchannel time shifts Δt_0 and Δt_1, it was necessary to interpolate the measured $I(t)$.

The model signal function $F(t)$ is fit to the data Y_n measured at discrete times t_n by varying parameters Y, τ, Δt_0, σ_0, Δt_1, and α. The maximum-likelihood fitting procedure for Poisson statistical uncertainties is used [28]: The estimator,

$$L_{\min} = \sum_n \{F(t_n) - Y_n \ln[F(t_n)]\}, \quad (3)$$

which is free from the approximation that the uncertainty distribution of the data is Gaussian, is minimized to obtain the best fit. The uncertainties of the parameters are obtained from the second numerical derivatives of $L_{\min}$ with respect to the parameters in the vicinity of the minimum.

Using the measured instrumental function and circular deconvolution method we were able to extract the parameters from the measured data. For a better visibility of the signal in a single 2-ns period, we have also tried to fold the signal of many bunches into an effective single-bunch signal by carefully choosing the time intervals and summing the data. With respect to the multibunch approach, the statistics of the signal increases, but so does the time jitter due to the folding algorithm. The extracted parameter σ_0 is found to be larger in the folded case, whereas the lifetime and its uncertainty remain practically the same (Fig. 3). In some cases, a fit analysis using the instrumental function did not return stable results. In these cases the decay signal of the very short-lived 8^+ state was used instead. The total uncertainty of the method was determined based on the fit uncertainty and the standard deviation of the extracted lifetimes around the average value in the cases, where no change of lifetime was expected. The overall uncertainty was determined to be in the 5-to-10-ps range.

The deconvolution method was verified by analyzing the time spectrum of the fluorescence decay of the He^+ $2p$ state, recorded just above the $N = 2$ threshold at the photon energy of 65.8 eV (Fig. 3). The lifetime was determined to be

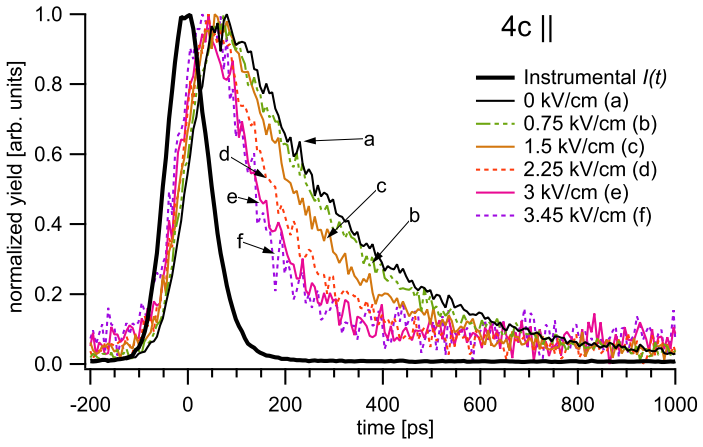

FIG. 4. (Color online) Influence of different field strengths on the decay time of the $4c$ state in parallel geometry ($\mathbf{F}||\hat{\mathbf{e}}_0$). The signal of different bunches has been folded into a single bunch and normalized to 1.

(101 ± 1) ps, which is in very good agreement with calculations and with the high-precision experimental value of 99.717 ± 0.075 ps [29].

III. THEORY

We compare the measured resonance lifetimes to the results obtained with our *ab initio* calculations. The singly excited and the doubly excited singlet states of the helium atom in an external dc electric field converging to the $N = 2$ ionization threshold have been calculated with the method of complex scaling (cf. [30–32] and the references therein). The method allows for the exact representation of resonance and continuum states using square-integrable basis sets. Only a brief outline of the calculation procedure is given here, and the reader is referred to Ref. [33] for details.

The complex-scaled Hamiltonian operator which describes the helium atom in the electric field is written as

$$H(\theta) = H_0(\theta) + \Delta H(\theta), \tag{4}$$

$$H_0(\theta) = e^{-i2\theta}\left(\mathbf{p}_1^2/2 + \mathbf{p}_2^2/2\right) + e^{-i\theta}(-2/r_1 - 2/r_2 + |\mathbf{r}_1 - \mathbf{r}_2|^{-1}), \tag{5}$$

$$\Delta H(\theta) = e^{i\theta}\, F(z_1 + z_2). \tag{6}$$

We denote the field-free Hamiltonian operator and the atom-field interaction with H_0 and ΔH, respectively, $\mathbf{r}_i$ and $\mathbf{p}_i$, $i = 1,2$, are the electron coordinates and momenta, and θ is the "rotation angle" [30–32]. The calculation of the eigenstates and the eigenenergies of $H(\theta)$ proceeds in two steps. In the first step, we seek the field-free solutions,

$$H_0(\theta)\Psi^0_{n\theta} = E^0_{n\theta}\Psi^0_{n\theta}, \tag{7}$$

where the wave functions $\Psi^0_{n\theta}(\mathbf{r}_1,\mathbf{r}_2)$ are expanded in a basis of configuration-interaction coupled two-electron Coulomb-Sturmian functions with two suitably chosen radial scaling parameters associated with the two electrons [33,34]. Our basis sets consist of the basis functions with the total angular momentum $L \leqslant 10$ of both odd and even parity π. For each value of the total momentum and parity, several pairs of radial scaling parameters are used. This allows us to obtain the field-free solutions within a single diagonalization for each L and π. In the second step, the solutions of

$$H(\theta)\Psi_{j\theta} = E_{j\theta}\Psi_{j\theta} \tag{8}$$

are sought, where a subset of the calculated field-free states is used to describe the wave functions $\Psi_{j\theta}$ [33]:

$$\Psi_{j\theta} = \sum_n y_{jn}\Psi^0_{n\theta} \quad (M_n = M_j). \tag{9}$$

In order to calculate the lifetimes of the DES considered in this work, their autoionization and radiative decay paths have been considered. The autoionization widths Γ^a_j are obtained from the imaginary parts of the complex energies $E_{j\theta} = E_j - i\Gamma^a_j/2$ associated with the resonance states $|\Psi_{j\theta}\rangle$. For these resonance states, the radiative decay widths Γ^r_j have been obtained by means of [33]

$$\Gamma^r_j = \frac{\alpha^3}{2\pi}{\sum_k}' \sum_\beta \int d\Omega\,(E_j - E_k)^3 \times \mathrm{Re}\,\{[\langle\overline{\Psi_{k\theta}}|D_\theta(\hat{\mathbf{e}}_\beta)|\Psi_{j\theta}\rangle]^2\}, \tag{10}$$

where $D_\theta(\hat{\mathbf{e}}_\beta) = e^{i\theta}\,\hat{\mathbf{e}}_\beta \cdot (\mathbf{r}_1 + \mathbf{r}_2)$ is the length-gauge dipole operator and the notation $\langle\overline{\Psi_{k\theta}}|$ means that the deconjugated radial part of the complex-scaled wave function is used under the integral. In Eq. (10), β runs over the two linearly independent polarizations of the emitted photon, and the prime denotes the summation over the singly excited states only since the transitions to the DES contribute negligibly to Γ^r_j compared to the transitions to the singly excited states. Furthermore, in order to avoid errors stemming from inaccurately calculated higher-lying singly excited states, only transitions to the singly excited states with principal quantum numbers $n \leqslant 18$ have been considered. Finally, the lifetimes reported here are calculated as

$$\tau_j = t_U/\left(\Gamma^a_j + \Gamma^r_j\right), \tag{11}$$

where $t_U \approx 2.418\,88 \times 10^{-17}$ s is the atomic unit of time.

IV. RESULTS AND DISCUSSION

In Fig. 5, the calculated lifetime dependence on the field strength is compared to the measured values for $nc\ ^1P^o$ $(n = 3$–$7)$ states. The agreement between the two is good for both relative orientations of the field and for the field strengths up to 3.5 kV/cm. While the $3c$ lifetime is practically independent on the field strength and its direction, the effect of the field is clearly seen for the states with $n \geqslant 4$: A

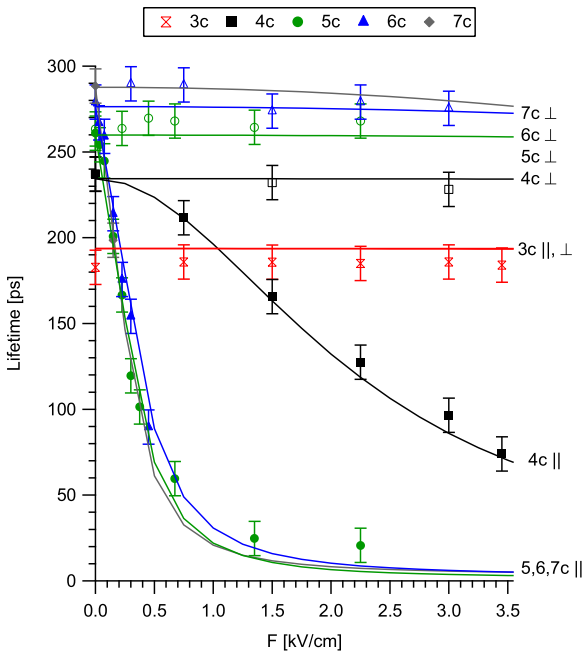

FIG. 5. (Color online) The lifetimes of the $nc\ ^1P^o$ resonances in the external electric field for the parallel ($\mathbf{F} \parallel \hat{\mathbf{e}}_0$) and perpendicular ($\mathbf{F} \perp \hat{\mathbf{e}}_0$) geometries. The measured lifetimes (points) are compared to the calculated results (lines).

TABLE I. The calculated energy differences $\Delta E_{ij} = E_i - E_j$ (in meV) and radiative (Γ^r) and Auger (Γ^a) decay rates of the $nc\ ^1P^o$ (A), $nb\ ^1S^e$ (B), and $(n+1)a\ ^1S^e$ (C) resonances in zero electric field (in atomic units). The last row gives the coefficient k in units of $(\mathrm{kV/cm})^{-2}$ obtained by fitting the theoretical data with ansatz (17). The numbers in the parentheses denote the powers of ten.

n	3	4	5	6	7
ΔE_{AB}	26.93	2.71	−0.39	−0.76	−0.68
ΔE_{AC}	−60.11	−25.26	−12.96	−7.54	−4.77
Γ^r_A	1.15(−7)	9.87(−8)	9.07(−8)	8.61(−8)	8.32(−8)
Γ^a_B	7.469(−5)	4.624(−5)	2.985(−5)	1.999(−5)	1.388(−5)
Γ^a_C	4.920(−4)	2.186(−4)	1.135(−4)	6.592(−5)	4.154(−5)
k	1.34 (−4)	0.189	10.9	8.23	14.1

considerable lifetime shortening is observed in the $\mathbf{F} \parallel \hat{\mathbf{e}}_0$ case when the field strength is increased. The calculations suggest that for $n \geqslant 4$ the Stark mixing with the strongly autoionizing $(n+1)a$ and $nb\ ^1S^e$ states [33,35] is responsible for this effect, as well as for quenching of the $nc\ ^1P^o$ fluorescence yield; for $n = 3$ the spacing between the states is too large for a significant mixing (see Table I), so that the lifetime is rather independent from the field strength. For $n \geqslant 4$ the quenching results mostly from the larger autoionization decay probability, since according to the calculations, the radiative widths of the $nc\ ^1P^o$ states are practically independent of the field strength in the investigated range. The effect appears mostly through the $nc\ ^1P^o$ -$nb\ ^1S^e$ Stark coupling: Despite the fact that the autoionization rate of the $nb\ ^1S^e$ states is about four times weaker compared to the $(n+1)a\ ^1S^e$ states, the $nb\ ^1S^e$-$nc\ ^1P^o$ energy difference is much smaller than the $(n+1)a\ ^1S^e$ -$nc\ ^1P^o$ energy difference (Table I). On the other hand, for the perpendicular setup, the lifetimes and fluorescence photon yields are found to be practically independent of the field strength and, as noted before in the zero-field regime [19,20], the lifetimes of the $nc\ ^1P^o$ states are observed to increase slowly with n.

Since the state's lifetime and its fluorescence yield depend on the same Stark coupling, measuring both as functions of the electric field strength provides additional information. For a given state, these two quantities are extracted from the fit [Eq. (1)] of the time spectra recorded at different field values F. In Fig. 6, the relative lifetime $\tau(F)/\tau(0)$ is plotted against the relative fluorescence yield $Y(F)/Y(0)$ for the $4c\ ^1P^o$ state in the parallel field configuration. As noted, these two quantities assume about the same value at the selected field strength. This result is consistent with a simple two-state mixing model presented below.

In the two-step absorption-emission model the relative fluorescence yield is related to the relative lifetime of an intermediate state by

$$\frac{Y(F)}{Y(0)} = f(F)\frac{\tau(F)}{\tau(0)}, \tag{12}$$

where

$$f(F) = [\sigma(F)/\sigma(0)][\Gamma^r(F)/\Gamma^r(0)]. \tag{13}$$

Above $\sigma(F)$ and $\Gamma^r(F)$ is the photoexcitation cross sections and the fluorescence decay rate, respectively, of an

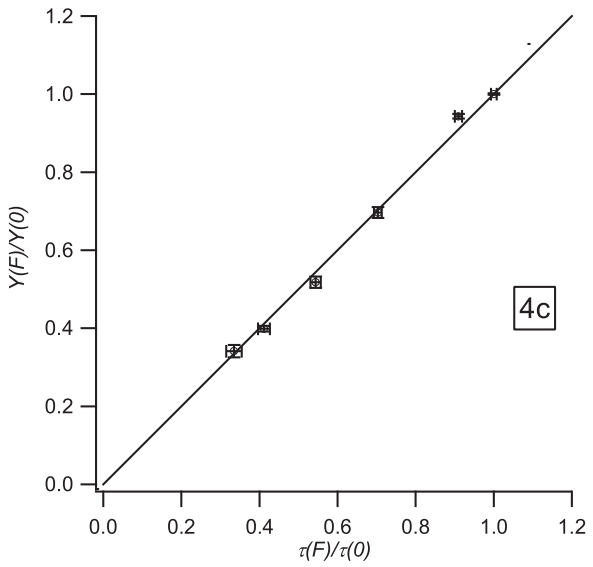

FIG. 6. The relative change of the signal amplitude versus the relative change of the lifetime as a function of electric field strength [Eq. (12)] for the $4c\ ^1P^o$ state.

intermediate state. Suppose that a "doubly visible" state $|A\rangle$ (meaning that the state can be photoexcited in the zero field and that it decays primarily by the fluorescence rate Γ^r, the $nc\ ^1P^o$ state) is Stark-mixed with a "doubly invisible" state $|B\rangle$ (a state which cannot be photoexcited when $F = 0$ and which decays primarily by autoionization rate Γ^a, the $nb\ ^1S^e$ state). The states are mixed upon application of an external field:

$$|A'\rangle = c_1(F)|A\rangle + c_2(F)|B\rangle, \tag{14}$$

$$|B'\rangle = c_2(F)|A\rangle - c_1(F)|B\rangle. \tag{15}$$

The field-dependent coefficients c_1 and c_2 may be assumed to be real without the loss of generality. As $c_1^2 = 1 - c_2^2$, the photoabsorption cross section of the state $|A'\rangle$ is simply $\sigma(F) = \sigma(0)[1 - c_2^2(F)]$ and similarly the fluorescence rate is $\Gamma^r(F) = \Gamma^r(0)[1 - c_2^2(F)]$. From these equations follows $f(F) = [1 - c_2^2(F)]^2$. This quantity is a measure for the Stark mixing coefficient c_2^2 and can be determined from the measured results by a presentation as given in Fig. 6. When $|c_2| \ll 1$, as realized in Fig. 6, it follows that $f(F) \approx 1$, and the relative fluorescence yield dependence on the electric field strength is practically the same as the relative lifetime dependence on F:

$$\frac{\tau(F)}{\tau(0)} = \frac{1}{1 + (\Gamma^a/\Gamma^r - 1)c_2^2(F)}. \tag{16}$$

Expressing c_2 by the first-order perturbation theory and taking into account that $\Gamma^a/\Gamma^r \gg 1$, Eq. (16) is written as

$$\frac{\tau(F)}{\tau(0)} \approx \frac{1}{1 + kF^2}. \tag{17}$$

The same parametrization form remains valid if other doubly invisible states contribute to the Stark mixing. Actually, the form (17) perfectly reproduces the theoretical curves with k values reported in Table I. The mixing coefficients calculated by means of the perturbation theory for field strengths above

2 kV/cm can surpass 0.1, which means that the first-order perturbation applicability is at its limit [26]. A hint about the real value of mixing coefficient in the two-state model is obtained from our nonperturbative calculations. For the parallel setup, the fluorescence decay rate is calculated to increase slightly with respect to the zero-field value. Taking 2.0% increase for the $6c\ ^1P^o$ state at $F = 3$ kV/cm, the corresponding mixing coefficient $c_2 \approx 0.14$. In the perpendicular geometry, the fluorescence rate is almost independent of the field strength.

According to theory, a mixing with the $^1D^e$ states is not forbidden in the perpendicular configuration. It is, however, notable only for $n \geqslant 7$ and explains the decreasing lifetime for $7c$ perpendicular in Fig. 5. At 3 kV/cm it causes a 2.8% decrease of the zero-field $7c\ ^1P^o$ lifetime. The effect of this mixing in the parallel geometry goes in the opposite direction, causing 1.3% increase of the lifetime at the same field strength.

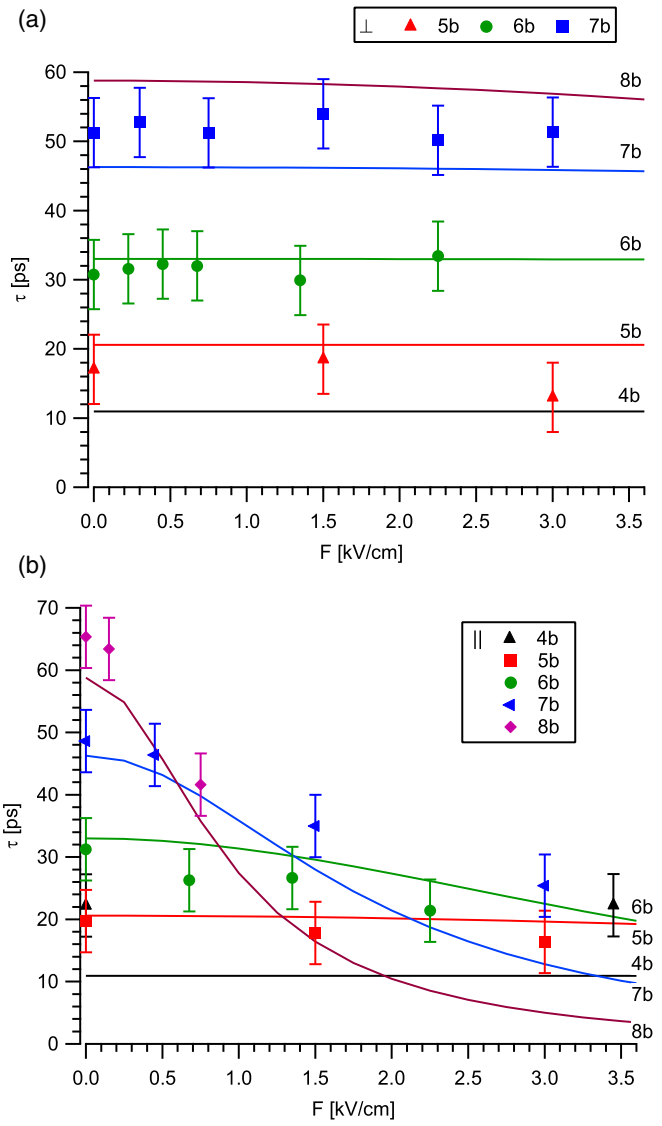

FIG. 7. (Color online) The lifetimes of the $nb\ ^1P^o$ resonances in the external electric field for the perpendicular ($\mathbf{F} \perp \hat{\mathbf{e}}_0$, a) and parallel ($\mathbf{F} \parallel \hat{\mathbf{e}}_0$, b) geometries. The measured lifetimes (points) are compared to the calculated results (lines).

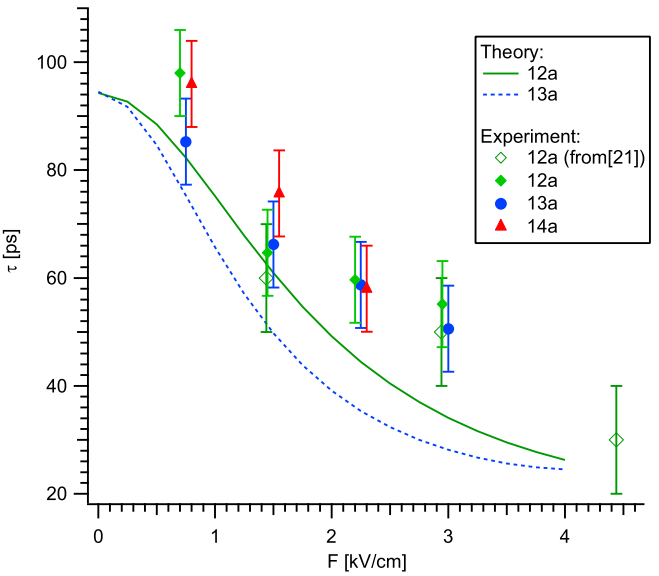

FIG. 8. (Color online) The lifetimes of the $na\ ^1P^e$ resonances in the external electric field for the perpendicular ($\mathbf{F} \perp \hat{\mathbf{e}}_0$) geometry. The measured lifetimes (points) are compared to the calculated results (lines), as well as the results from [21]. The points are shifted horizontally for clarity to avoid overlapping.

Note that $nb\ ^1S^e$ energy jumps over the $nc\ ^1P^o$ energy when n changes from 4 to 5. This is reflected in the local maximum of k at $n = 5$, as seen in Table I.

The lifetime dependence on the dc electric field has been measured also for the $nb\ ^1P^o$ ($n = 4$–8) and $2pnp\ ^1P^e$ ($n = 12$–14) resonances (Figs. 7 and 8). The latter case deals with a series of dark resonances of even parity which become visible at high n due to the Stark mixing with the autoionizing $^1P^o$ series, as mentioned above. The observed shortening of the lifetime is in agreement with the previous results [21]. For the dipole-allowed $nb\ ^1P^o$ resonances the theory predicts the lifetimes to increase from 11 to 60 ps when n increases from 4 to 8 [36]. These lifetimes are too short to be precisely measured with our present time resolution of about 10 ps and too long to be accurately extracted from the measured spectral linewidth. It is interesting to compare our results with the results in [2], where the linewidths were extracted from the fit of the resonance profiles in the experimental photoionization spectrum. The linewidths extracted from our measurements in the time domain are 0.030(10) and 0.033(10) meV, for the $4b\ ^1P^o$ and $5b\ ^1P^o$ states, respectively, while the corresponding values from [2] are 0.06(2) and 0.03(3) meV. Similar to its close neighbor state $(n-1)c\ ^1P^o$, the lifetime of the $nb\ ^1P^o$ resonance remains stable as the field strength increases in the perpendicular orientation and diminishes for the parallel field orientation due to the Stark mixing with $(n-1)b\ ^1S^e$ and $na\ ^1S^e$ resonances. We note that the $nb\ ^1P^o$ states are more stable than the neighboring $(n-1)c\ ^1P^o$ states because a stronger mixing is required to quench the fluorescence signal of the predominantly autoionizing $nb\ ^1P^o$ resonances.

V. CONCLUSIONS

We have measured the lifetimes of the helium DES $nc\ ^1P^o$ ($n = 3$–7), $nb\ ^1P^o$ ($n = 4$–8), and $na\ ^1P^e$ ($n = 12$–14)

with dc electric fields strengths up to 3.5 kV/cm for the parallel and perpendicular field orientations with respect to the incoming photon polarization. The experiment was performed in the multibunch mode of the synchrotron radiation facility BESSY II to allow for accumulation of a statistically relevant set of data at energy resolution sufficiently high to fully resolve the signal of the $7c$-$8b\ ^1P^o$ doublet (separated by 2 meV). The zero-field data confirm the results of previous measurements on $nc\ ^1P^o$, as well as the results regarding the lifetimes of the $na\ ^1P^e$ states in a weak electric field. Increasingly strong fluorescence quenching is observed for predominantly fluorescing $n = 3$–7 series of $nc\ ^1P^o$ states in the parallel field orientation, while for the perpendicular field orientation, the fluorescence yield remains practically independent of the electric field. This is explained by Stark mixing with the dipole-forbidden predominantly autoionizing $(n-1)b\ ^1S^e$ and $na\ ^1S^e$ states. Less intense, but similar in behavior and origin is the fluorescence quenching of the $nb\ ^1P^o$ ($n = 4$–8) series of states. The measured trends are well reproduced by calculations.

ACKNOWLEDGMENTS

This work is supported by Research Programme No. P1-0112 of the Slovenian Research Agency and by bilateral Project No. BI-FR07-PROTEUS-10 (14024HW).

[1] M. Domke, G. Remmers, and G. Kaindl, Phys. Rev. Lett. **69**, 1171 (1992).
[2] K. Schulz, G. Kaindl, M. Domke, J. D. Bozek, P. A. Heimann, A. S. Schlachter, and J. M. Rost, Phys. Rev. Lett. **77**, 3086 (1996).
[3] M. K. Odling-Smee, E. Sokell, P. Hammond, and M. A. MacDonald, Phys. Rev. Lett. **84**, 2598 (2000).
[4] J.-E. Rubensson, C. Såthe, S. Cramm, B. Kessler, S. Stranges, R. Richter, M. Alagia, and M. Coreno, Phys. Rev. Lett. **83**, 947 (1999).
[5] K.-H. Schartner, B. Zimmermann, S. Kammer, S. Mickat, H. Schmoranzer, A. Ehresmann, H. Liebel, R. Follath, and G. Reichardt, Phys. Rev. A **64**, 040501 (2001).
[6] M. Coreno, K. C. Prince, R. Richter, M. de Simone, K. Bučar, and M. Žitnik, Phys. Rev. A **72**, 052512 (2005).
[7] J. Söderström, M. Agåker, A. Zimina, R. Feifel, S. Eisebitt, R. Follath, G. Reichardt, O. Schwarzkopf, W. Eberhardt, A. Mihelič, M. Žitnik, and J.-E. Rubensson, Phys. Rev. A **77**, 012513 (2008).
[8] T. W. Gorczyca, J.-E. Rubensson, C. Såthe, M. Ström, M. Agåker, D. Ding, S. Stranges, R. Richter, and M. Alagia, Phys. Rev. Lett. **85**, 1202 (2000).
[9] F. Penent, P. Lablanquie, R. I. Hall, M. Žitnik, K. Bučar, S. Stranges, R. Richter, M. Alagia, P. Hammond, and J. G. Lambourne, Phys. Rev. Lett. **86**, 2758 (2001).
[10] J. G. Lambourne, F. Penent, P. Lablanquie, R. I. Hall, M. Ahmad, M. Žitnik, K. Bučar, P. Hammond, S. Stranges, R. Richter, M. Alagia, and M. Coreno, J. Phys. B **36**, 4339 (2003).
[11] J.-E. Rubensson, A. Moise, A. Mihelič, K. Bučar, M. Žitnik, and R. Richter, Phys. Rev. A **81**, 062510 (2010).
[12] A. Mihelič, M. Žitnik, K. C. Prince, M. Coreno, and R. Richter, Phys. Rev. A **85**, 023421 (2012).
[13] M. Ström, C. Såthe, M. Agåker, J. Söderström, J.-E. Rubensson, S. Stranges, R. Richter, M. Alagia, T. W. Gorczyca, and F. Robicheaux, Phys. Rev. Lett. **97**, 253002 (2006).
[14] J. R. Harries, J. P. Sullivan, J. B. Sternberg, S. Obara, T. Suzuki, P. Hammond, J. Bozek, N. Berrah, M. Halka, and Y. Azuma, Phys. Rev. Lett. **90**, 133002 (2003).
[15] C. Såthe, M. Ström, M. Agåker, J. Söderström, J.-E. Rubensson, R. Richter, M. Alagia, S. Stranges, T. W. Gorczyca, and F. Robicheaux, Phys. Rev. Lett. **96**, 043002 (2006).
[16] K. C. Prince, M. Coreno, R. Richter, M. de Simone, V. Feyer, A. Kivimäki, A. Mihelič, and M. Žitnik, Phys. Rev. Lett. **96**, 093001 (2006).
[17] S. I. Fedoseenko, D. V. Vyalikh, I. E. Iossifov, R. Follath, S. A. Gorovikov, R. Püttner, J. S. Schmidt, S. L. Molodtsov, V. K. Adamchuk, W. Gudat, and G. Kaindl, Nucl. Instrum. Methods Phys. Res., Sect. A **505**, 718 (2003).
[18] J. G. Lambourne, F. Penent, P. Lablanquie, R. I. Hall, M. Ahmad, M. Žitnik, K. Bučar, M. K. Odling-Smee, J. R. Harries, P. Hammond, D. K. Waterhouse, S. Stranges, R. Richter, M. Alagia, M. Coreno, and M. Ferianis, Phys. Rev. Lett **90**, 153004 (2003).
[19] F. Penent, J. G. Lambourne, P. Lablanquie, R. I. Hall, S. Aloïse, M. Žitnik, K. Bučar, and P. Hammond, AIP Conf. Proc. **697**, 151 (2003).
[20] J. R. Harries, J. P. Sullivan, and Y. Azuma, J. Phys. B **37**, L169 (2004).
[21] M. Žitnik, F. Penent, P. Lablanquie, A. Mihelič, K. Bučar, R. Richter, M. Alagia, and S. Stranges, Phys. Rev. A **74**, 051404 (2006).
[22] L. Lipsky, R. Anania, and M. J. Conneely, At. Data Nucl. Data Tables **20**, 127 (1977).
[23] C. D. Lin, Phys. Rev. A **29**, 1019 (1984).
[24] J.-M. Rost, K. Schulz, M. Domke, and G. Kaindl, J. Phys. B. **30**, 4663 (1997).
[25] M. Žitnik, K. Bučar, M. Štuhec, F. Penent, R. I. Hall, and P. Lablanquie, Phys. Rev. A **65**, 032520 (2002).
[26] M. Žitnik and A. Mihelič, J. Phys. B: At., Mol. Opt. Phys. **39**, L167 (2006).
[27] N. H. Gale, Nuclear Physics **38**, 252 (1962).
[28] J. G. Lambourne, Ph.D. thesis, University of Manchester, 2001.
[29] G. W. F. Drake, J. Kwela, and A. van Wijngaarden, Phys. Rev. A **46**, 113 (1992).
[30] A. Buchleitner, B. Grémaud, and D. Delande, J. Phys. B **27**, 2663 (1994).
[31] Y. K. Ho, Phys. Rep. **99**, 1 (1983).
[32] N. Moiseyev, Phys. Rep. **302**, 212 (1998).
[33] A. Mihelič and M. Žitnik, Phys. Rev. Lett. **98**, 243002 (2007).
[34] G. Lagmago Kamta, B. Piraux, and A. Scrinzi, Phys. Rev. A **63**, 040502 (2001).
[35] A. Bürgers, D. Wintgen, and J.-M. Rost, J. Phys. B **28**, 3163 (1995).
[36] A. Mihelič, Ph.D. thesis, University of Ljubljana, 2006.